Journal Pre-proof

Groundwater potential zones identification using geoelectrical sounding and remote sensing in Wadi Touil plain, Northwestern Algeria

Mohand Bersi, Hakim Saibi

PII: S1464-343X(20)30265-X

DOI: https://doi.org/10.1016/j.jafrearsci.2020.104014

Reference: AES 104014

To appear in: *Journal of African Earth Sciences*

Received Date: 3 May 2020

Revised Date: 15 September 2020

Accepted Date: 23 September 2020

Please cite this article as: Bersi, M., Saibi, H., Groundwater potential zones identification using geoelectrical sounding and remote sensing in Wadi Touil plain, Northwestern Algeria, *Journal of African Earth Sciences* (2020), doi: https://doi.org/10.1016/j.jafrearsci.2020.104014.

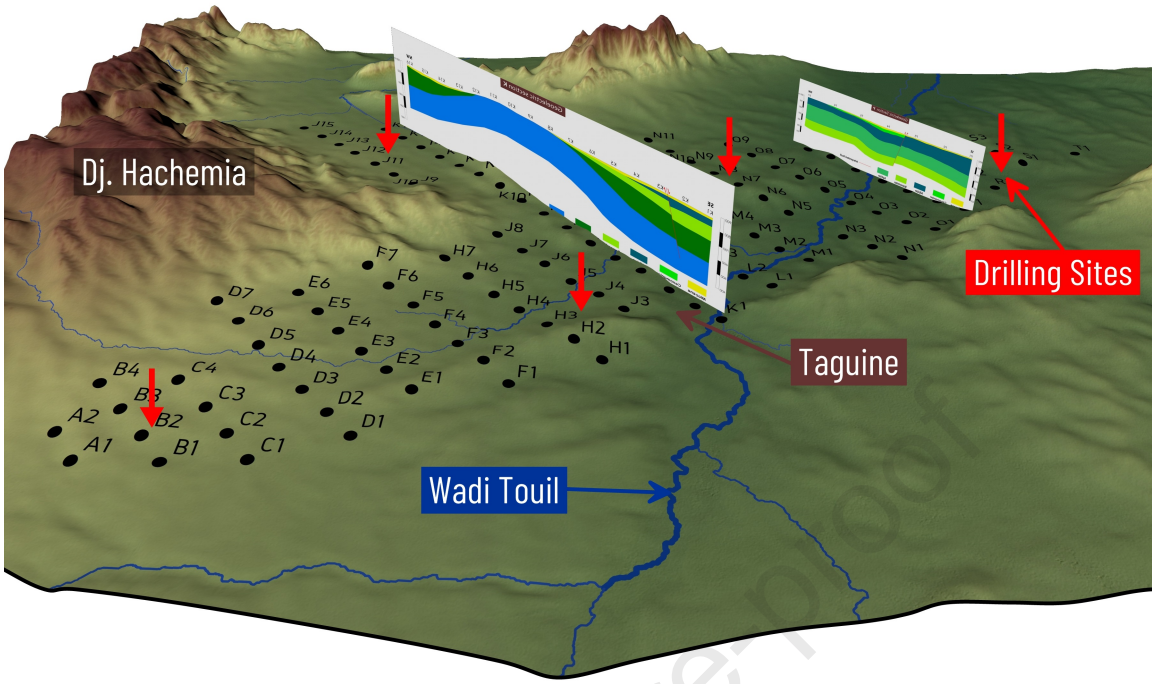

Groundwater potential zones identification using geoelectrical sounding and remote sensing in Wadi Touil plain, Northwestern Algeria

Mohand Bersi[a*], Hakim Saibi[b]

[a] Department of Earth Sciences, Ferhat Abbas University, Sétif, Algeria. ORCID: 0000-0003-2608-3871

[b] College of Science, Geology Department, United Arab Emirates University. ORCID: 0000-0001-8803-6945, saibi.hakim@gmail.com / hakim.saibi@uaeu.ac.ae

Corresponding Author: Dr. Mohand Bersi: E-mail: (mbersi@hotmail.fr)

Address: Department of Earth Sciences, Ferhat Abbas University Setif 1, 19000 El Bez Campus, Setif, Algeria.

Abstract

The Wadi Touil plain is situated southwest of Tiaret city; it contains two important localities, Ksar Chellala (Reibell) and Zemalet El Amir Abdelkader (Taguine). This semi-arid region belongs to the western high plains and is characterized by scarce and irregular rainfall. The lack of surface water and the agricultural activities of this region increase the demand for groundwater. Several water boreholes were installed to meet the large water needs; however, these boreholes no longer cover the high demand for water due to the increase in population, increase in irrigated areas, and wear and tear on pumps. Therefore, in order to better define the catchment area and find new sites that meet the water quality and quantity requirements, a geoelectrical survey using the electrical resistivity method was carried out in the Wadi Touil large plain South of Tiaret to investigate the electrical characteristics of sub-surface layering and evaluate the aquifer potentials. Using the Schlumberger array, a total of 127 vertical electrical soundings were conducted along 16 profiles. The recorded data were interpreted quantitatively and qualitatively through the use of isoapparent resistivity maps, geoelectrical pseudo-sections analysis, and the established geoelectric sections. The results show the presence of three very promising levels; the surface aquifer formed by the Mio-plio-Quaternary terrain (ρ = 55 ohm.m), the Barremian-Albian-Aptian complex (ρ = 300 ohm.m), and the Jurassic aquifer (ρ = 1200 ohm.m). In this study, we determined the extent of these aquifers, their depth and their thickness. These results provide a better understanding of the geology and the deep geo-structure of the region. The remote sensing observations using Sentinel 2A images located the wet lands and provided visual evidence of the evolution of the irrigated areas over time. Finally,

according to the study results, the most favorable sites for the establishment of water exploitation boreholes are proposed.

Keywords: Geoelectrical investigation; Arid regions; Water supply; Groundwater aquifers; Northwestern Sahara Aquifer System (NWSAS); Sentinel 2A

1. Introduction

Groundwater is the main source of supply for people in arid and semi-arid areas. It forms a perennial reserve to which people lean during water crises and periods of drought. The large underground water reservoirs in arid and semi-arid regions of Algeria have experienced depletion of their resources in recent years; this is mainly due to the high demand to support the expansion of irrigated areas (Famiglietti, 2014). The study area belongs to the western high plains in northwest Algeria, which is a part of the Northwestern Sahara Aquifer System (NWSAS). The NWSAS is dealing with a negative balance between aquifer recharge and water exploitation leading to a crucial depletion (Richey, 2014). Overexploitation of groundwater also contributes to the deterioration of water quality through increasing saltiness (Custodio, 2002; Khezzani and Bouchemal, 2018; Mamou et al., 2006). The high plains region has experienced a large increase in cultivated areas thanks to a development plan for these regions in the Algerian government's 2010-2015 five-year plan (Mozas and Ghosn, 2013). Hence, more water is pumped, leading to the depletion of surface aquifers. The authorities have launched a geophysical prospecting campaign using the geoelectric method in the Wadi Touil large plain, with the aim of satisfying the needs of the growing populations, notably those of Ksar Chellala and Taguine. These two agglomerations are situated in the Wadi Touil large plain characterized by high evapotranspiration (Fatah et al., 2012; Hamimed et al., 2008; Laouisset and Dellal, 2016), which increases the demand for water.

The study area belongs to the semi-arid climate zone characterized by hot summers and cold winters. The annual rainfall in the Wadi Touil region rarely exceeds 300 mm/year. This low precipitation rate is insufficient to effectively recharge shallow aquifer resources. The geomorphological aspect of the study area allows gathering waters from the surrounding mountains. The Wadi Touil large plain receives high flows from the Djebel Hachemia and Southern Atlas Mountains of the Aflou region. This water accumulates over the Wadi Touil and contributes to the water table recharge in addition to the annual rainfall directly in the Wadi Touil large plain.

During the geoelectric campaign carried out by the national geophysical company (ENAGEO) in the Wadi Touil region, 127 vertical electrical soundings were conducted along 16 profiles using the Schlumberger array (Fig. 1). This method is proven to be a low-cost technique and verifiable tool in groundwater exploration, especially for hydrogeological surveying of arid and semi-arid areas (Asfahani, 2007b; Nejad et al., 2011). Thus, several geophysical studies by electrical survey have been carried out in similar regions to solve water-related problems (Kosinski and Kelly, 1981; Yadav and Singh 2007; Sikandar and Christen, 2012; Maury and Balaji, 2014) and investigate deep underground aquifers (Aoudia et al., 2020; Metwaly et al., 2012; Asfahani, 2007a; Asfahani, 2013; Zaidi and Kassem, 2012; Redhaounia et al., 2015).

The recorded data were interpreted by establishing isoapparent resistivity maps for different AB (depth), analyzing the geoelectrical pseudo-sections (apparent resistivity) and establishing geoelectric sections (true resistivity). The results revealed the existence of three potentially aquifer levels: (i) The mio-plio-quaternary aquifer with limited resources, (ii) The continental intercalary (CI) formed by the formations of the Albian, Barremian, Aptian and Neocomian, and (iii) The Jurassic aquifer, essentially karstic. The geoelectric sections show that the CI has good characteristics of hydraulic continuity and thickness. Moreover, the geoelectric results indicate the existence of structural discontinuities oriented NE-SW, which are interpreted as faults and these faults seem to be controlling the subsurface water gradient. Consequently, the Sentinel 2A images show that the eastern part of the Wadi Touil plain is more humid and contains more plant cover than the western part.

The different maps and results were integrated and overlain in a geographic information system (GIS) to locate the suitable areas for catchment drilling and to more clearly identify the deep geological structure of the study area that may control the aquifer flow paths of the region.

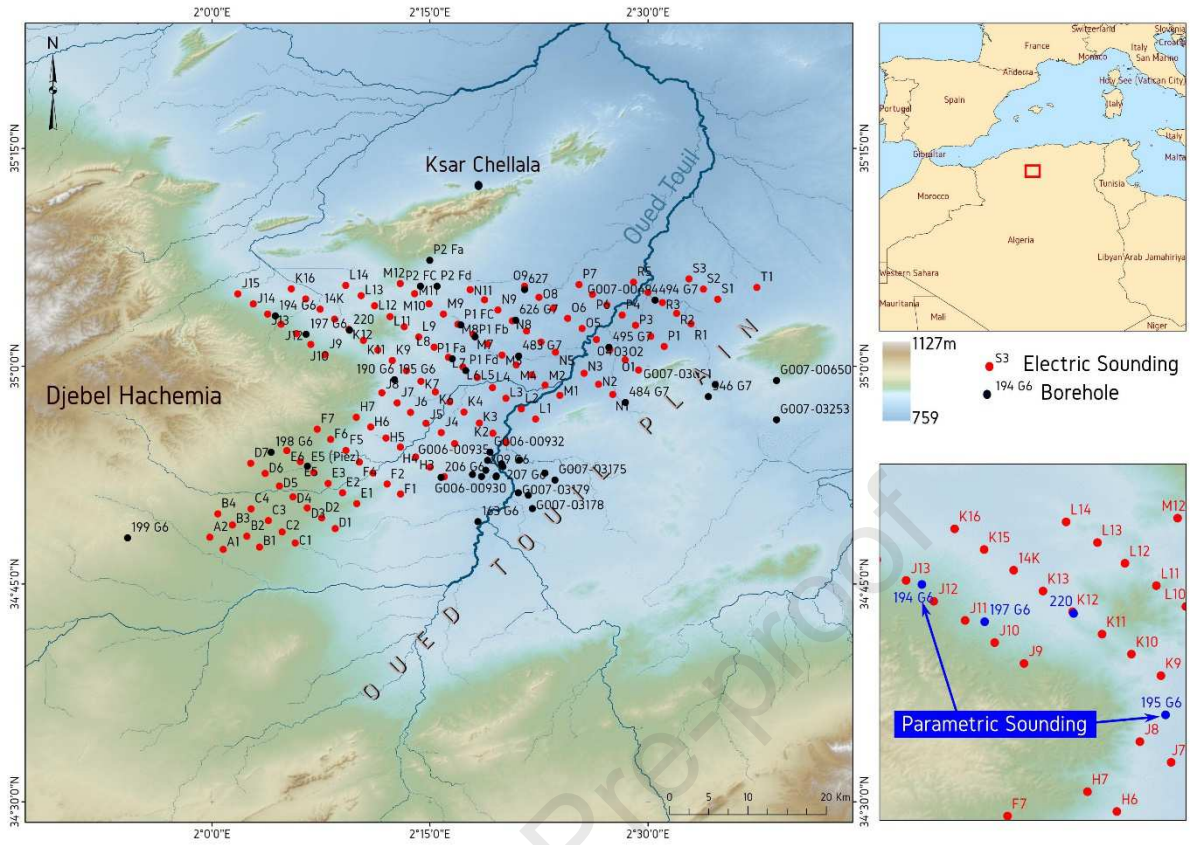

Fig. 1 General location map of the Wadi Touil plain showing the vertical electrical soundings location.

2. Geology and hydrogeology

The study area belongs to the western Saharan Atlas where the sedimentary cover contains formations ranging from the Jurassic to the Quaternary. The lithology and ages of formations have been recognized from outcrops and drilling. The geological work undertaken in the study area is primarily discussed in mission reports (Ayad, 1991; Ayad, 1997; Braham and Hamidouche, 2007; Cornet, 1954; Caratini, 1970). The most important part of the study area is covered by Tertiary fill, which unconformably overlies the Cretaceous and Jurassic formations. The tertiary fill is formed by Miocene sandstones and Pliocene-Quaternary sands and clays. The thickness of this level ranges from 1 to 100 m with an average thickness of 25 m. Hydrogeologically, this level contains limited water resources; nevertheless, a hundred traditional wells produce the waters of this aquifer. Thus, we consider this level an important aquifer for domestic and pasturage purposes.

The Cretaceous age formations form the important layers in thickness. These formations outcrop in the northeastern part of the study area. The Turonian outcrops on both sides of the Wadi Touil at the latitude of the small town of Taguine (Fig. 2). The Turonian is formed by massive, sometimes fractured limestones. It has secondary porosity from cracks and karst cavities, which gives it water aquifer potential. However, in our study

area it is thinner; hence, it is not considered an important aquifer resource in this region. The Cenomanian is mainly marl and outcrops around the Faidh Es Snak area. The thickness of this level is large and therefore very important, up to 500 m. Although large, this the Cenomanian rock unit is characterized by a low permeability and poor water production potential. The Albian outcrops in Douar Megane in the south and in Faidh Es Senak in the northeast and is an important aquifer in the Atlas region (Maoui et al., 2010; Kerbadj et al., 2017; Edmunds et al., 2003; Winn, 1973). It is mainly sandstones with very good hydrodynamic characteristics; its thickness is around 300 m. The Aptian unit is important in the Wadi Touil plain, despite its not outcropping, but its underground extension is important. The Aptian is an average thickness of 250 m and forms, with the Barremian and the Albian levels, the well-known CI aquifer. The CI aquifer has an average thickness of 1000 m and contains the Barremian sandstones, which are great than 400 m thick. This aquifer has an impermeable substratum formed by limestones and marly dolomites. These impermeable levels with approximately 130 m thickness, are attributed to the Neocomian.

Jurassic formations outcrop in the anticline structure of Djebel Hachemia. The deep borehole (194 G6, see Fig. 1) indicates the presence of two levels, the first consists of the Portlandian, which is 270 m thick and mainly clay and limestone. This level is characterized by a low permeability. The second level is the Kimmeridgian, which is formed by fractured dolomites and limestones. The total thickness of the Kimmeridgian formation is 350 m, which is an important karstic aquifer.

The study area is within the western Saharan Atlas, which is an intercontinental mountain range in North Africa. The structures in this region are elongated in a NE-SW direction (Amri et al., 2017). The major faults in the western Saharan Atlas are NE-SW trending normal faults (Bracène and de Lamotte, 2002). Wadis often border these faults when they are extensive and active. The small faults contribute to the aquifer recharge; especially in the Jurassic outcrops where the faults network is well developed.

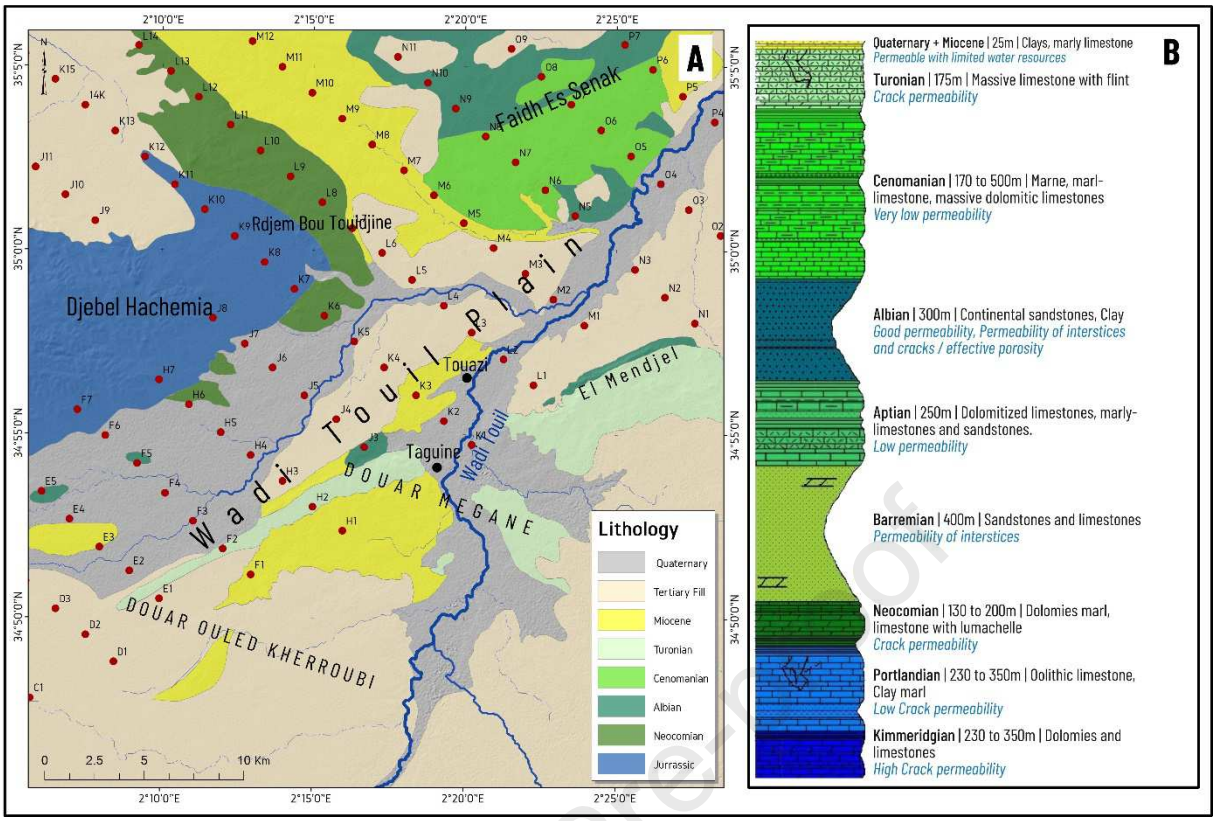

Fig. 2 A Geological map of the study area, modified after (modified from Cornet (1954)), B: Synthetic stratigraphic log. .

3. Materials and Methods

3.1. Vertical Electrical Soundings (VES)

ENAGEO carried out a geophysical campaign in 1987 using the vertical electrical survey method in the Wadi Touil plain. The Schlumberger electrode configuration having a maximum current electrode spread AB of 4000 m was used and performed using the Scintrex TSQ-3 transmitter. A total of 127 surveys using the Schlumberger array configuration were collected (Fig.3). Briefly, a vertical electrical sounding is represented by a discrete sequence of apparent resistivity measures of the subsurface, carried out with a growing spacing between a couple of current electrodes (A and B) (Cimino et al., 2007) . In the Schlumberger array, the apparent resistivity is calculated according to the equation:

$$\rho_a = k\frac{\Delta V}{I}$$

126 Where: $k = \pi \frac{(\frac{AB}{2})^2 - (\frac{MN}{2})^2}{MN}$, $\Delta \boldsymbol{V} = potential\ difference$ and $\boldsymbol{I}$ = current intensity

127

128 Fig. 4 shows the basic principles of an electrical method survey. The data collected during this mission were
129 used by the National Agency for Hydraulic Resources (ANRH) for drilling projects. Through this study, we use
130 recent software and methods to further refine and re-interpret the VES data.

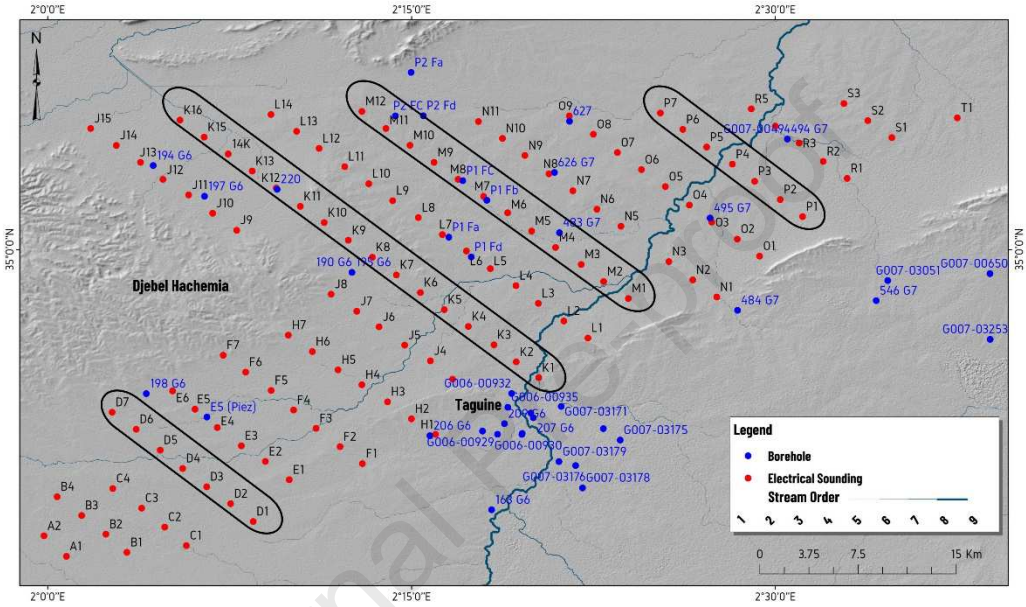

131

132 **Fig.3** Distribution map of the vertical electrical soundings and boreholes in the study area.

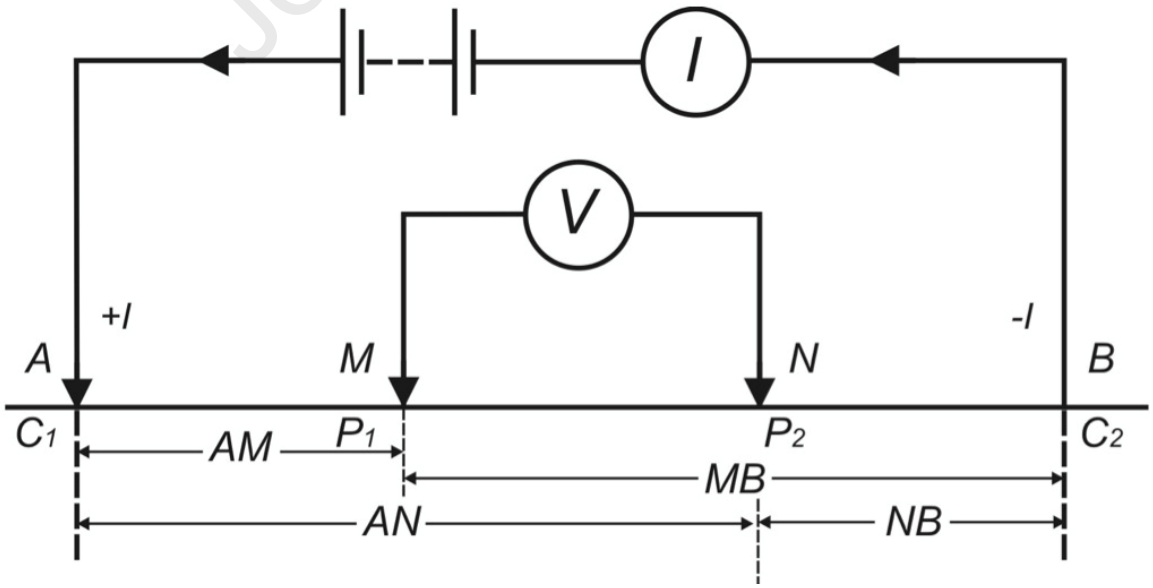

133

Fig. 4 Principle of electrical method. Electrical current is injected at A and B electrodes. Difference in potential is measured between M and N electrodes.

The raw data were used to develop isoapparent resistivity maps and pseudo electric sections. The apparent resistivity curves were obtained and interpreted using the IPI2WIN software, and then results were used to calibrate the true resistivities with borehole data to obtain the resistivity scale. Four boreholes named 194-G6, 195-G6, 495-G7 and 627-G7 located very close to VES sites named J13, K8, O4 and O9, respectively (Fig. 1). Through the IPI2WIN software we calculated resistivity curves as a function of the depth; that is, a real terrain resistivity with respective depth. Then, we compared the depth given by the software and that of the stratigraphic log of the well (we chose the four most complete logs). The O4 VES is situated in the Wadi Touil valley. The resistivity curve indicates the presence of three geoelectric layers, which are interpreted from the stratigraphic log of 495-G7 borehole as three geological units. Hence, the first layer with a resistivity of 85.4 Ohm.m and thickness of 4.89 m, was attributed to the Quaternary (Fig. 2), the second layer was attributed to a resistant Cretaceous level (Albian sandy aquifer), and a third layer was attributed to a conductive Cretaceous level (Aptian). Similarly, the other VES resistivities were calibrated with the respective boreholes (Fig. 5). A synthetic stratigraphic and corresponding resistivity scale was established to better interpret the geoelectric sections and pseudo-sections (Fig. 6).

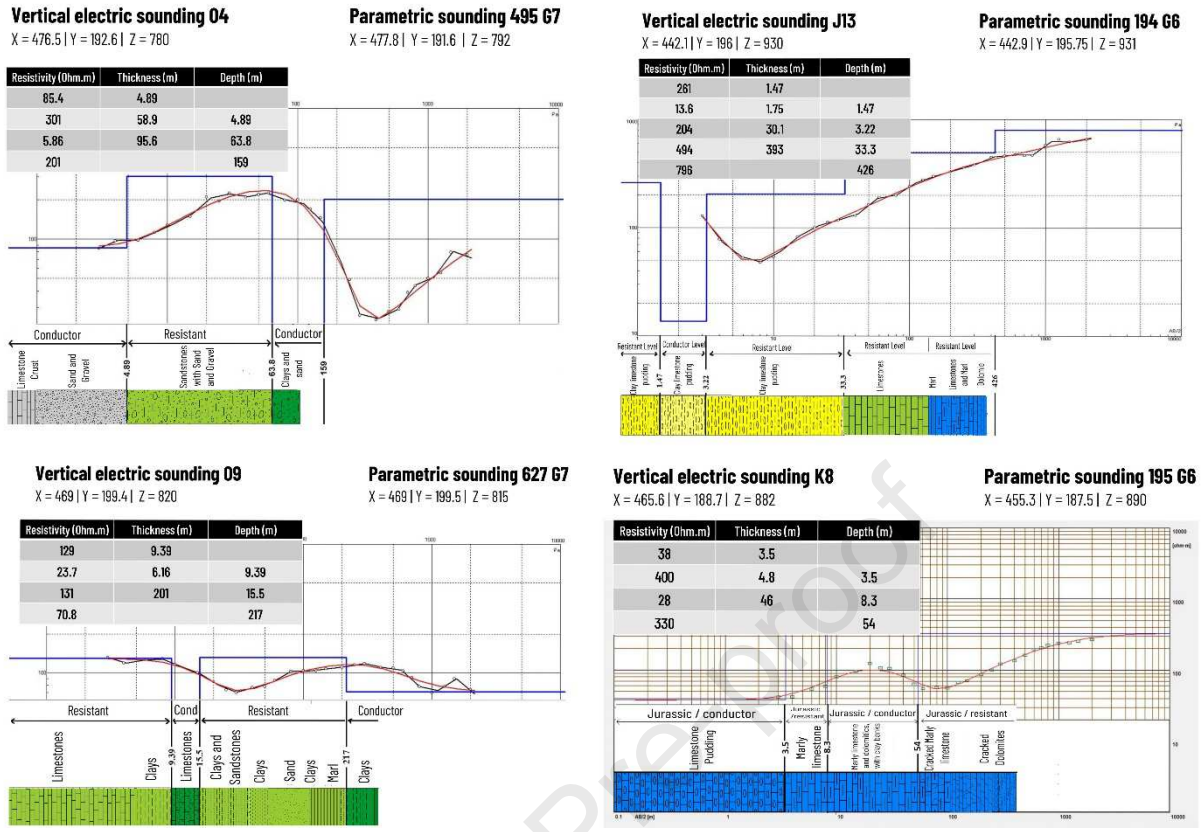

Fig. 5 Calibration of four standard VES surveys using four boreholes.

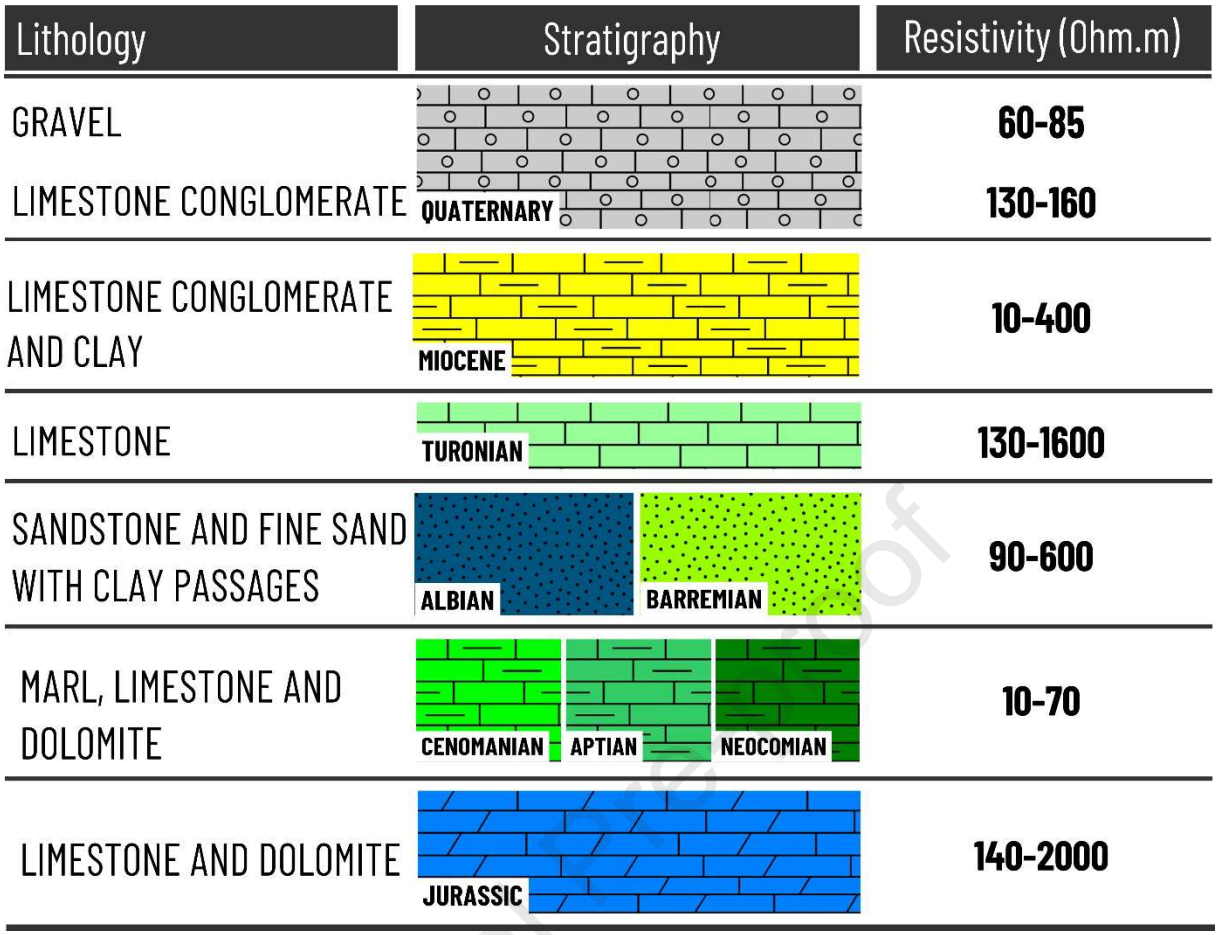

Fig. 6 Synthetic resistivity scale in the study area.

According to the resistivity scale, the geoelectrical sections were realized and interpreted. Using the geoelectrical sections, pertinent information (depth, thickness and longitudinal conductance) about promising layers was collected and organized in a data base. From these, aquifer characteristics maps were produced.

3.2. Remote sensing

Two remotely sensed data sets were used to map the evolution of agricultural and vegetated lands from 2001 to 2018. These consist of the Sentinel 2A data set and the LandSat 7 Enhaced Thematic Maper ETM. The Sentinel 2A image (Tile T31SDU) was recorded November 21st, 2018 and downloaded for free from https://scihub.copernicus.eu. The Landsat 7 ETM + image (Row 36, Path 196) recorded April 16th, 2001 was downloaded for free from https://www.earthexplorer.usgs.gov. The two images were processed using ARCGIS software. The applied image processing techniques are band ratios and Principal Component Analysis (PCA).

The band ratio technique consists of dividing one spectral band by another band. It facilitates differentiation between land cover types (Madani and Emam, 2011). The PCA is a method in which original data is transformed from a large dataset in six spectral bands into a compressed representation in a few new bands, here, the three first neo-bands, called principal components (Torbick and Becker, 2009). These two techniques are widely used in geosciences as a tool to map geological features, land use and land cover, water bodies, etc., (Gad and Kusky, 2007; Bersi et al., 2016; Saibi et al., 2018; Chabane et al., 2019; Lasaponara, 2006; Mohamed et al., 2018). The results of these two techniques produced values for the total vegetated and irrigated agricultural lands during the respective time periods, which we then used to make a land use comparison between the time periods. The Sentinel image allowed us to detect an underground water barrier which manifests at the surface as a discontinuity in the vegetation cover.

Both the VES technique and remote sensing contribute additional understanding of the water potential of the study area. The VES technique allows investigating the subsurface potential zones and detect the saturated layers, while the remote sensing technique detects the shallower humid zones, which indicates the presence of a source of underground water. Therefore, the coupled techniques produce a best practice for locating promising groundwater drilling target zones. Finally, a general map showing the suitable sites for new water drilling is presented. The methodological approach is summarized in Fig. 7.

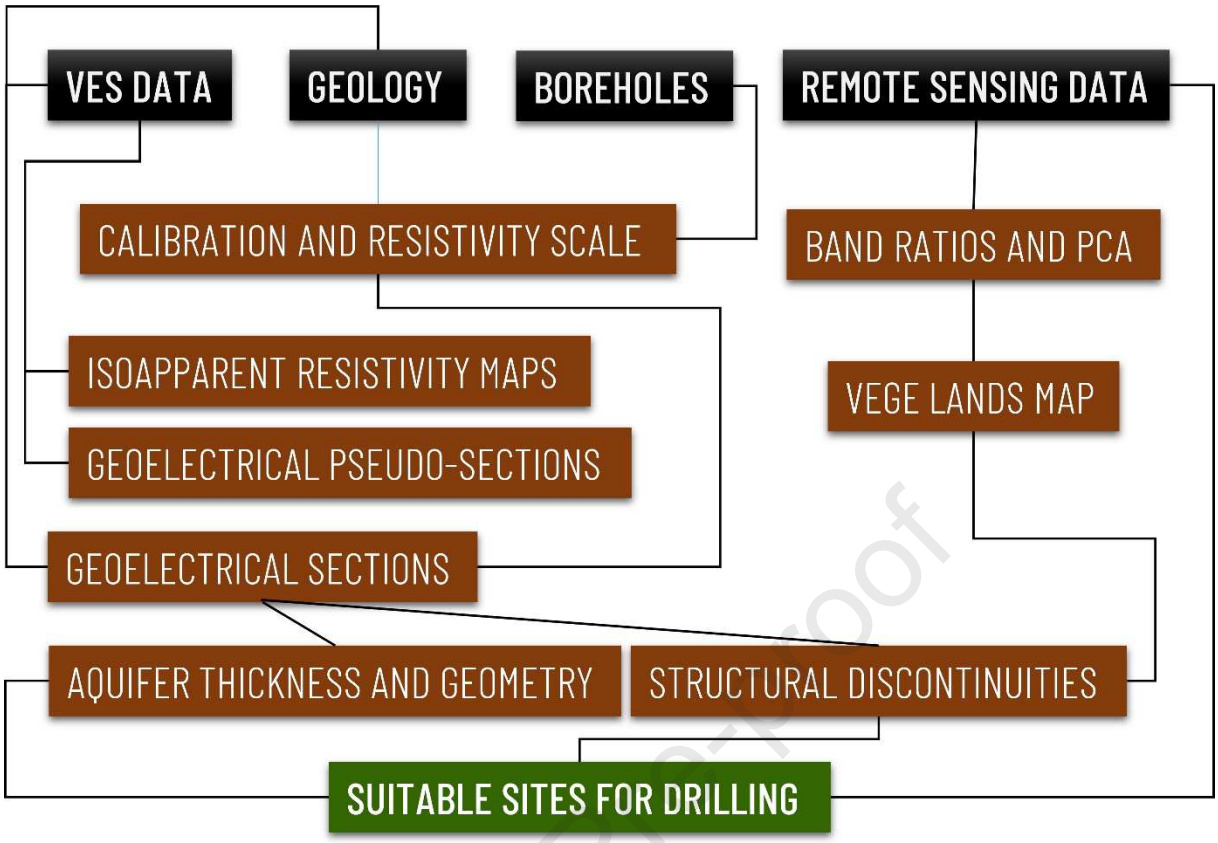

Fig. 7 Methodological approach.

4. Results and discussion

4.1. Isoapparent resistivity maps

ArcMap GIS software is used in this study to spatially represent the isoapparent resistivity of six different AB values. The depth of investigation depends on the distance between the two outside electrodes AB (Roy and Apparao, 1971). Thus, for the used Schlumberger array, the depth of investigation is of the order of 0.1 to 0.3 times the AB length (Barker, 1989; Roy and Elliot, 1981; Benabdelouahab et al., 20019). For this study, the average penetration depth is AB/4 (0.25 times AB length). Generally, the AB isoresistivity map shows facies variations that affect layers at depth between AB/4 and AB/5. The results from VES are used to plot isoapparent resistivity contour maps at AB = 200, 500, 1000, 2000, 3000 and 4000 m. Thus, the obtained maps are used to investigate terrains at 0 to 50, 50 to 125, 125 to 250, 250 to 500, 500 to 750 and 750 to 1000 m depth.

The AB = 200 m map shows the geological formations located at an approximate depth of 40 m (Fig.8). The resistivity ranges from 9.6 to 1120 Ohm.m. The low resistivity values are concentrated in the Wadi Touil valley,

north of Taguine locality. This area is characterized by thick Quaternary and Miocene sediments, which are very good conductors when relatively wet. The high resistivity values are concentrated in Djebel Hachemia (J9, J10 and J11 VESs), indicating a shallower Jurassic formation, and in Faidh Es Senak region (O8 VES) resulting from the Cenomanian thin layer (a resistant limestone). The high resistivity anomaly around S1 and S2 VESs is due to the high topographic position of these surveys, which is on the crest line (Redjem Amour) formed by the bulging of very resistant tertiary formations.

The AB = 500 m map shows the geological formations located at an approximate depth of 120 m. The resistivity ranges from 12.6 to 1370 Ohm.m and two anomalies were observed in this map. The first is a negative anomaly (low resistivity values) located along the Wadi Touil valley, which can be explained by the thickness of tertiary sediments in this valley and by the presence of underground waters which come from irrigation and waste waters. The positive anomaly (high resistivity values) is located in the Djebel Hachemia Jurassic anticline.

The AB = 1000, 2000 and 3000 m maps, which investigate layers at 200, 400 and 600 m depth, respectively, indicate the presence of a deep positive anomaly in Djebel Hachemia due to the massive Jurassic limestones and dolomites. While, the negative anomaly became larger and occupies the Wadi Touil plain, this can be explained by the presence of thick Cretaceous conductive layers (Neocomian). However, the Barremian-Albian and Aptian complex aquifer presents resistivities between 60 and 200 Ohm.m, and thus it is hard to separate between this aquifer and other deep cretaceous levels.

The AB = 4000 m map shows the deep structure of the study area around 1000 m depth. We observe two distinct resistivity zones; the western part is characterized by resistant material, which can be the extension of the Jurassic layers. The eastern part is characterized by conductive material, which can be explained by the thickness of soft cretaceous material in this region, a result of the regional dip.

The isoapparent resistivity maps show deep Jurassic material in the western part of the study area and deep, conductive cretaceous material in the eastern part. The two materials seem separated by structural discontinuities at different depths. These discontinuities may be normal faults forming a semi-graben, a common tectonic structure in the Atlas.

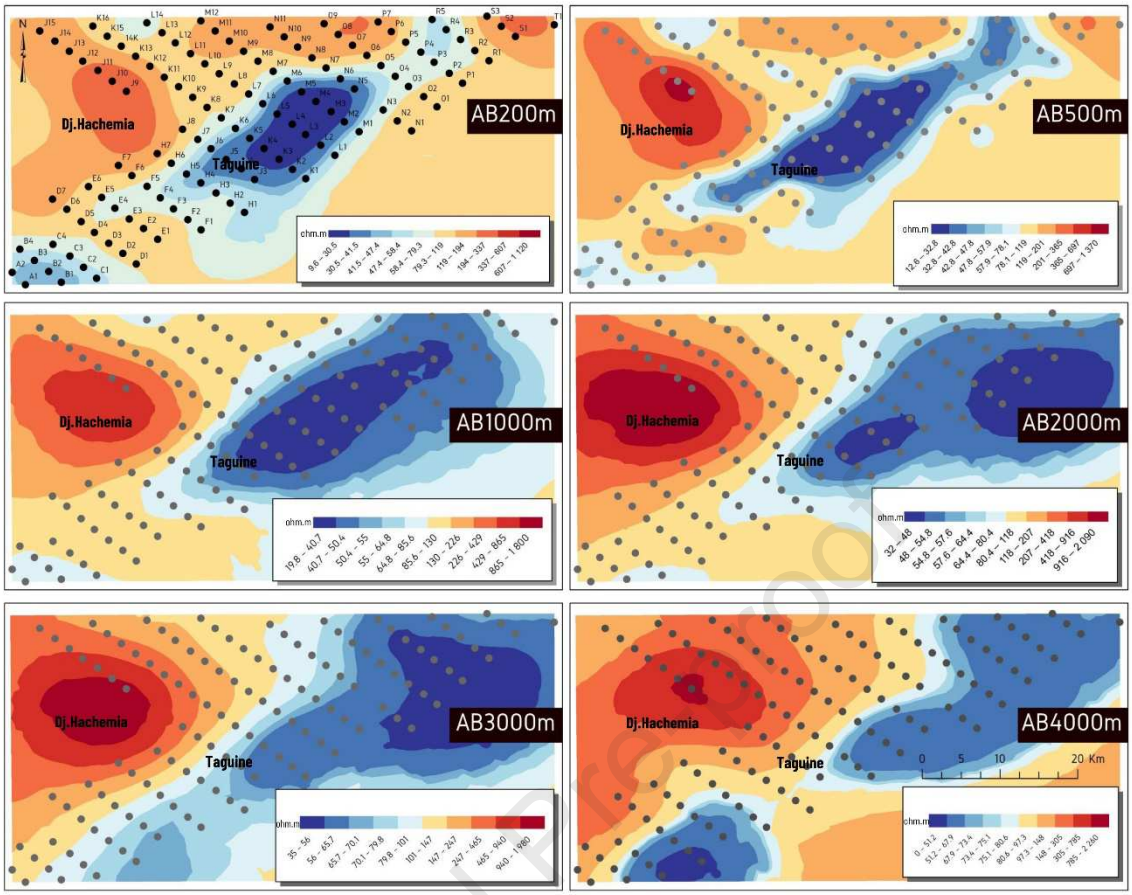

Fig. 8 Isoapparent resistivity maps showing the subsurface geo-electrical structure of the study area.

4.2. Pseudo sections and geoelectrical sections

The pseudo section reflects the apparent resistivity distribution as a function of electrode spacing versus (AB/2) values. The geoelectrical section reflects the true resistivity values in each sounding according to the depth (the section was plotted using the IPI-res3 tool of the IPI2WIN software). Thus, we join equal resistivity values to obtain and map a geological layer. The interpretation is according to the resistivity scale and drilling logs. The profiles D, K, M and P were selected for presentation regarding their strategic position and path. These are the only four pseudo sections and four geoelectrical sections presented at this time.

4.2.1. Profile D (Fig.3)

Pseudo section:

This pseudo section shows the presence of two very resistant zones; the first at the D2 and D3 soundings at an average depth (200 to 250m), may be due to the Turonian limestone layer buried between these two soundings.

237 This local anomaly may indicate the presence of two normal faults forming a grabben (Fig. 9). The second
238 resistant zone at D7 is deep and reflects the rise of Jurassic formations near the Djebel Hachemia anticline. The
239 conductive areas are likely the Cretaceous formations.

240 *Geoelectrical section*

241 Our interpretation of true resistivities along the D profile shows monoclinic layers with relatively large dips
242 between D5 and D6. In the southeast, the thickness of the Cretaceous layers is important to examine; their
243 thickness decreases going towards the NW where the Jurassic is less deep. The CI aquifer (Barremian-Albian-
244 Aptian) is significant from D1 to D3; the resistivities of these formations range from 134 to 177 Ohm.m.

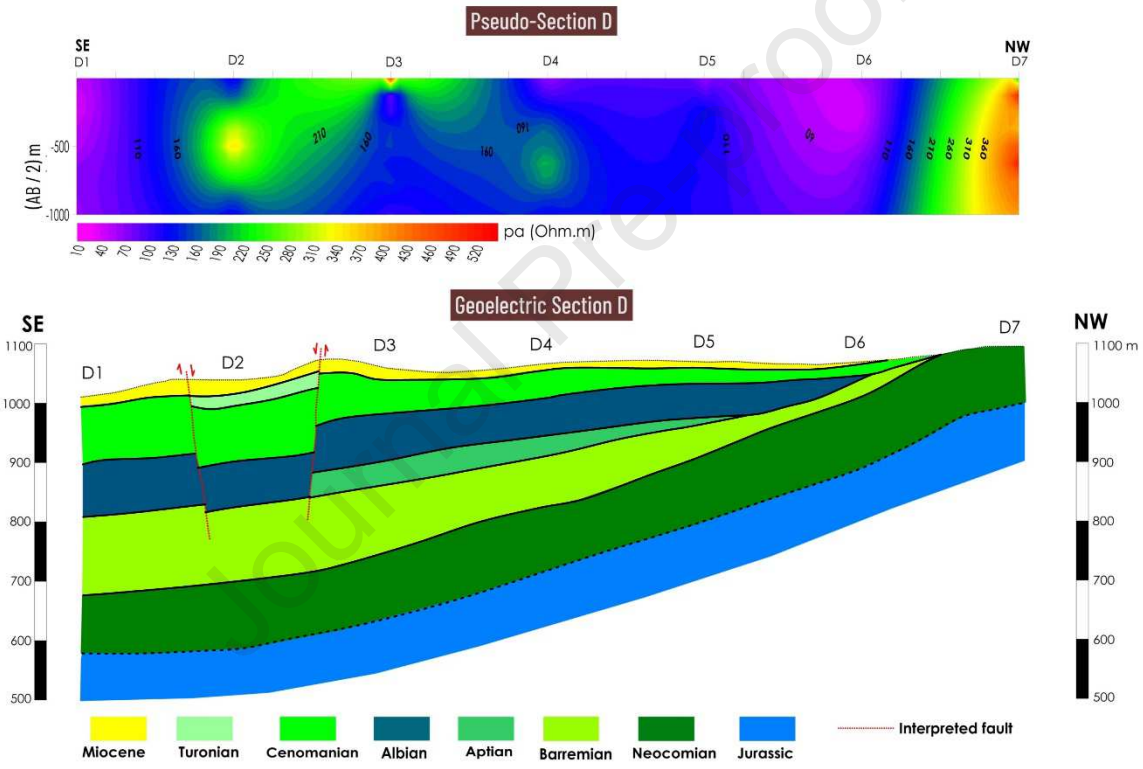

245

246 **Fig. 9** D profile pseudo section and geoelectrical section.

247

248 *4.2.2. Profile K*

249 *Pseudo Section*

250 This section shows two different resistivity zones; the first is resistant, appears from K7 to K13 and reflects the
251 Jurassic anticline at Djebel Hachemia. The second is conductive, appears from K1 to K6 and reflects the
252 Cretaceous formations.

Geoelectrical Section

The geoelectric section shows a shallower Jurassic substratum from K7 to K13 which consist of Jurassic limestones of the Djebel Hachemia Anticline (Fig. 10). The resistivity of this formation ranges from 103 to 1340 Ohm.m. The CI aquifer is thicker in the southeast, where the lateral changes in resistivity suggest the presence of a normal fault between K2 and K3. The CI formations along this section are limited to the Albian and Barremian with a reduced thickness and a resistivity ranging from 150 to 430 Ohm.m.

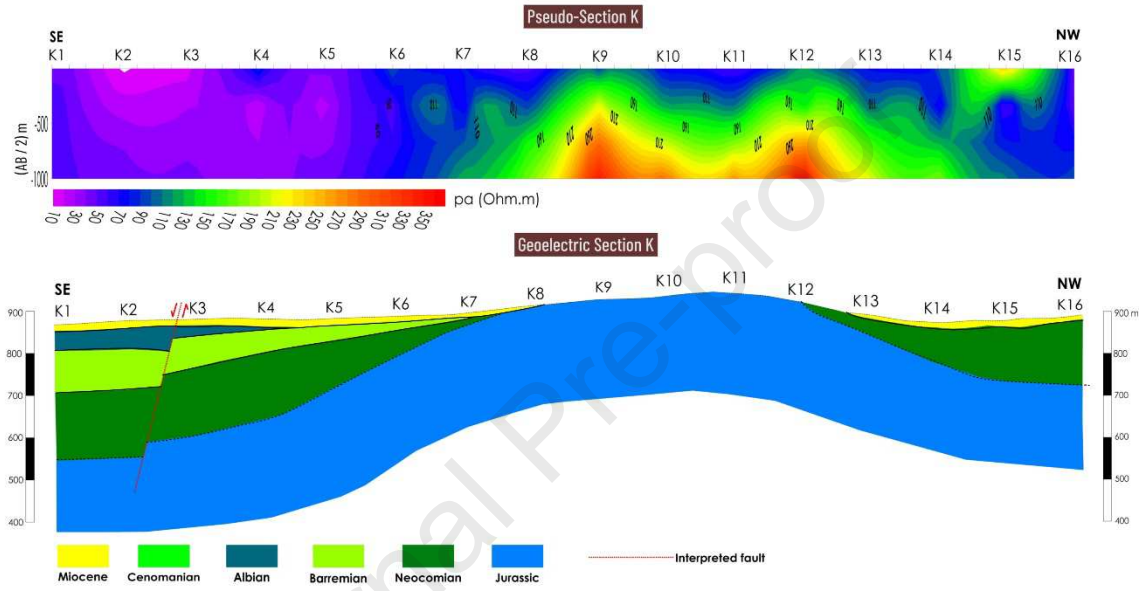

Fig.10 K profile pseudo section and geoelectrical section.

4.2.3. Profile M

Pseudo Section

This section is oriented NW-SE. The NW part is relatively resistant and it reflects a shallower resistant Jurassic substratum surmounted by the resistant Barremian layer. The SE part presents conductive layers with significant thickness. These conductive layers refer to the lower CI aquifer.

Geoelectrical section

The geoelectric section shows a large thickness of the CI aquifer, especially from the M1 to M7 soundings. The thickness becomes moderate after M7 where we interpret the presence of a normal fault. Another fault is interpreted between M2 and M3. The presence of this fault makes the thickness of the Cenomanian thin at M2

and M1. The geoelectric section also shows a shallower Jurassic substratum around M11 and M12, and becomes suddenly deeper at M10 (Fig. 11), Therefore, a fault is interpreted between M10 and M11.

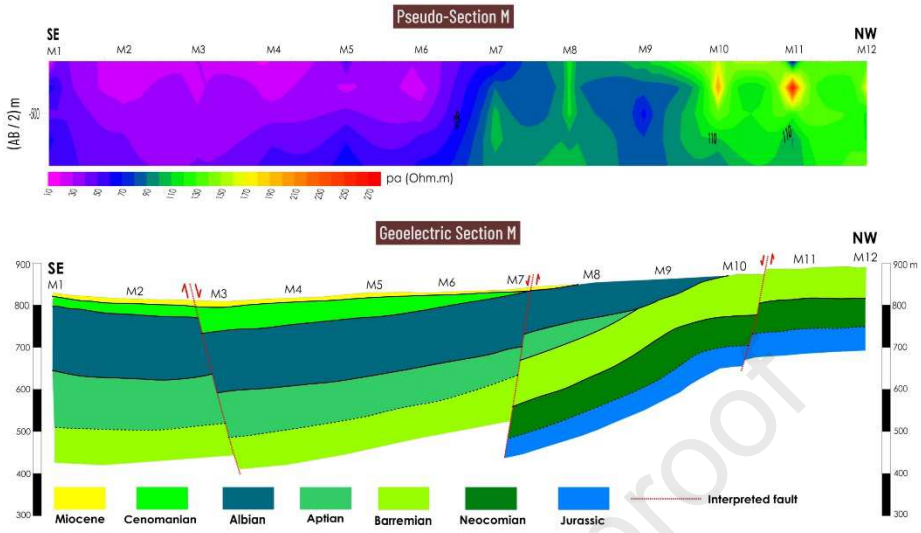

Fig. 11 M profile pseudo section and geoelectrical section.

4.2.4. Profile P

Pseudo section

The P profile pseudo section is characterized by a low, lateral variability of resistivity values, which is attributed to the relative horizontality of the layers and to the relatively uniform thicknesses.

Geoelectrical section

The geoelectrical section shows the continuous thick formation of the CI aquifer (Fig. 12). The Albian unit is thicker in the SE and becomes less thick from P4 to P7. Therefore, we interpret a fault between P3 and P4. The Barremian substratum is relatively resistant, from 117 to 274 Ohm.m.

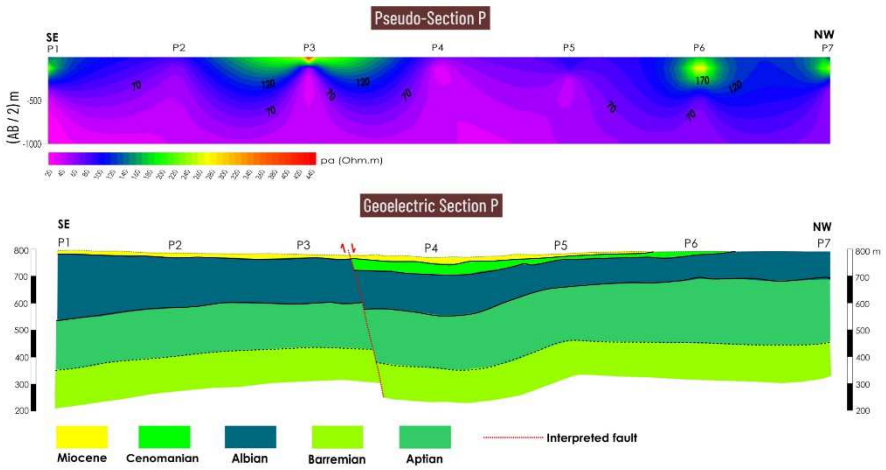

284

285 **Fig. 12** P profile pseudo section and geoelectrical section.

286

287 **4.3. The isodepth and isopach maps of the Albian and Barremian Aquifers**

288 Determining the thickness and depth of the Albian and Barremian layers forming the CI aquifer is a very
289 important step in understanding their geometry and their potential. In each survey in the geoelectrical sections,
290 the depth and thickness of the layer (Albian and / or Barremian) were extracted. Then, isodepth and isopach
291 maps were produced for the two layers (Fig. 13).

292 The Albian is most shallow in soundings J3, O1, O2 and P7, while it is generally shallower in the northeast and
293 deeper in the southwest (Fig. 13a). The average depth is 54 m which is a good indication regarding the drilling
294 cost. The thickness of the Albian is variable from 5 to 250 m, with an average thickness of 135 m. The most
295 significant thicknesses are located in soundings P1, S2, O7, O8, O9 and N11 in the northeast and in D1, D2, B3
296 and B4 in the southwest. The thinner areas are in K1, K2, N1, N2, O2 and E3 (Fig. 13b).

297 The Barremian aquifer is deeper (average depth 205 m) and relatively thicker (average thick 173 m) than the
298 Albian aquifer. The depth of this aquifer is greater in the northeast (200 to 550 m) and shallower in the southwest
299 along J, K and L profiles (Fig. 13c). The Barremian is thick in the northeast and thin in the southwest. The
300 greatest thickness is around soundings S2, S3, R2 and R3 (Fig. 13d).

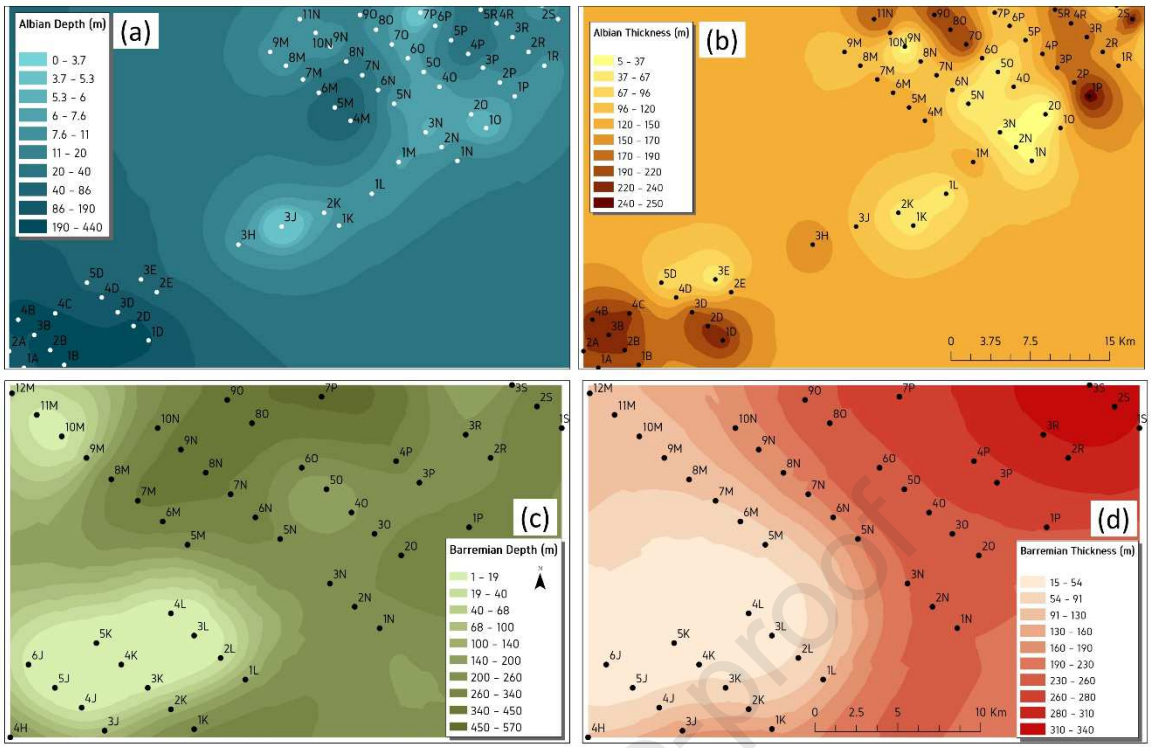

Fig. 13 Isodepth and isopach maps of Albian and Barremian aquifers. A) Isodepth map of the Albian aquifer. B) Isopach map of the Albian aquifer. C) Isodepth map of the Barremian aquifer. D) Isopach map of the Barremian aquifer.

The combination of depth and thickness is used to determine the best aquifer potential zone; this idealized zone must be at medium depth (> 50m) to avoid pollution and surface salinity and must be of a good thickness (> 100m) to ensure a water resource quantity usable for the medium and long term. Therefore, we used the depth divided by thickness for the two aquifers to locate the suitable zones of best aquifer geometry. Zones located in P1, P7, O7 to O9, N9 to N11, J3 and H3 are the most promising Albian zones (Fig. 14). Other zones can also be good aquifers regarding their large thicknesses, although they are relatively deeper and may be more expensive to drill. The promising Barremian zones are located in S3, P3, M9 to M12, K3 to K5 and L2 to L3. Similarly, other promising areas exist deeper and thicker with good water resources for which the drilling costs will be more expensive along P, O, R and S profiles.

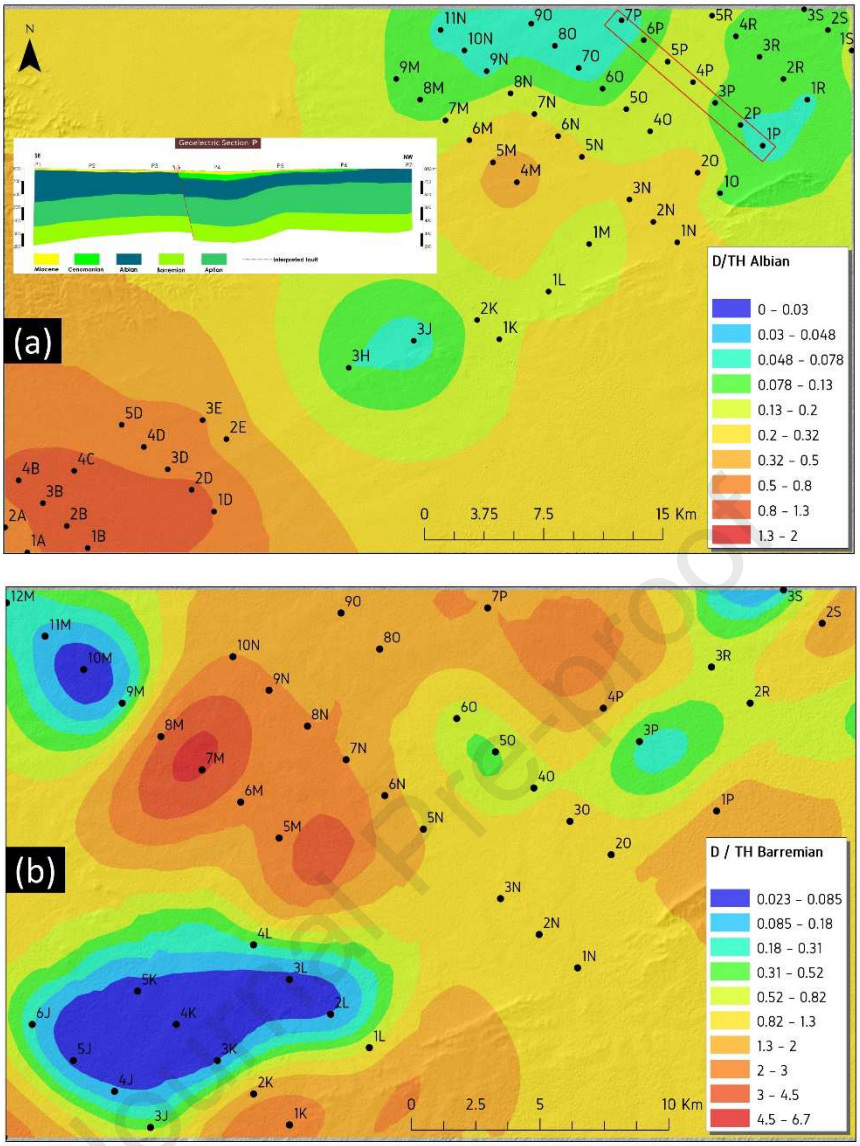

315

316 **Fig. 14** Best aquifer geometry and promising zones.

317

318 **4.4. Remote sensing**

319 Remote sensing techniques are increasingly used in earth sciences. Remote sensing data, especially
320 multitemporal, data provide information on changes undergone by the earth's surface. The multispectral data
321 from Sentinel 2A and LandSat 7 ETM sensors were used to map the change in irrigated areas from 2001
322 (LandSat Data) to 2018 (Sentinel 2A Data). The two image processing techniques ratioing and PCA were
323 utilized. These two techniques are widely used for land use change detection purposes. The PCA was applied to
324 the six multispectral bands of the LandSat 7 image and the equivalent bands in the Sentinel 2A image. The
325 newly obtained bands (components) contain different information where the first three components contain more

than 98% of the total information. Therefore, these three components were selected to display in RGB mode (Fig. 15). The PCA map shows a net increase of vegetation cover from 2001 to 2018, even though the 2001 image was taken in April, which is a rainy period in the study area. The map also shows a concentration of green lands on the eastern side of Wadi Touil, which can be explained by the presence of a long fault separating the eastern side from the western side. The presence of dense healthy green vegetation in the eastern part can be explained by the presence of a shallower water source. This source presumably feeds the vegetation during the dry seasons. In contrary, in the western part, the groundwater source is deeper because of the fault, as indicated by the low vegetation density. The interpreted fault may be at the origin of the wadi path and play the role of underground obstacle for water circulation. Additionally, farmlands increase in the study area in 2018; some of these farmlands are cultivated and appear in dark green (irrigated areas). Note that the large water body in the map is the Zahrez Gharbi Chott, which is a depression containing saline water and cannot play a role in the development of irrigated areas right now, unless a desalination system is installed.

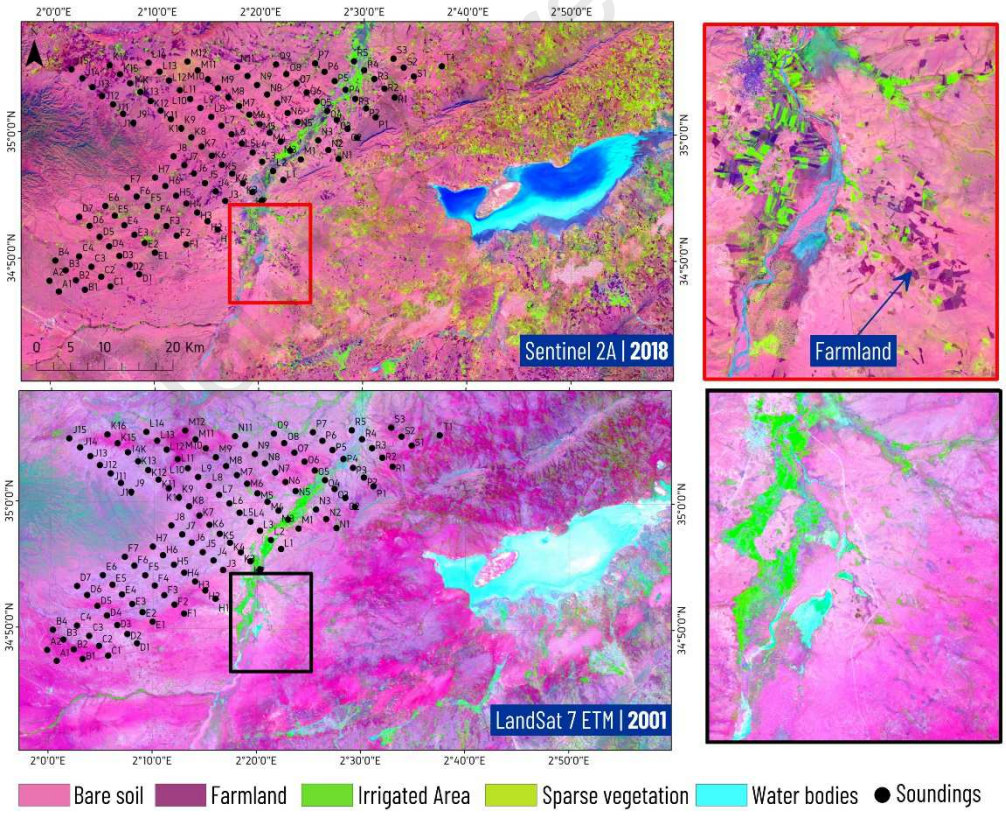

Fig. 15 PCA map showing vegetation density and repartition in 2001 and 2018.

The ratioing technique applied to Red and Near Infrared (NIR) bands in both images consists of dividing the red band by the NIR band. Vegetation is identified by the high absorption of electromagnetic energy in the red domain, and also by the high reflectance in the NIR domain. So, by dividing red band by NIR band, we obtain very low values on vegetation cover (0.2 to 0.5), which are well separated from other land covers. The analysis of the ratio map for both dates and images is used to assess the evolution of irrigated areas from 2001 to 2018. We observe the repartition of irrigated zones over the eastern side of the study area. These zones are important in 2018 because of the local development that this region experienced in the last decade (Fig. 16). The deep boreholes are located in the western side of the study area, which confirms the unequal underground water gradient. The traditional wells are located near the Taguine locality where the sources are shallower.

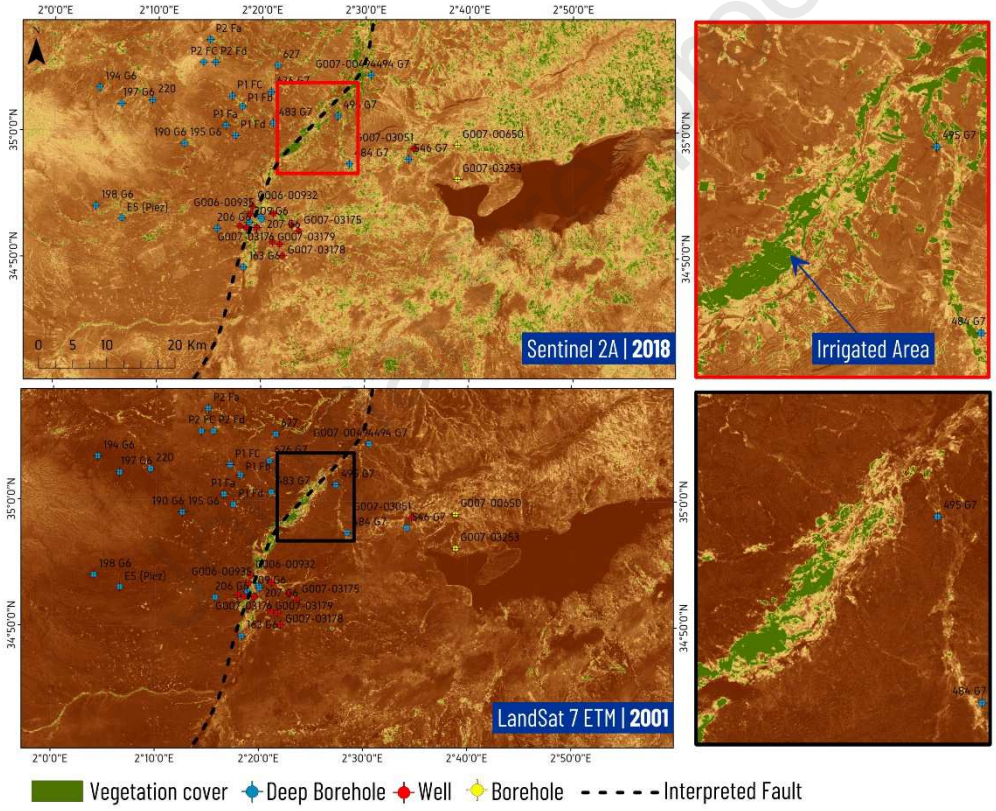

Fig. 16 Red/NIR Ratios map showing irrigated areas.

4.5. Favorable areas for drilling

the most suitable zones for drilling are identified for the study area following the VES and remote sensing results and interpretations. The most important areas for the CI and Jurassic aquifers are presented (Fig. 17), although

more areas may be favorable for drilling projects (Tertiary, Turonian and Neocomian), but with lower, limited production potential.

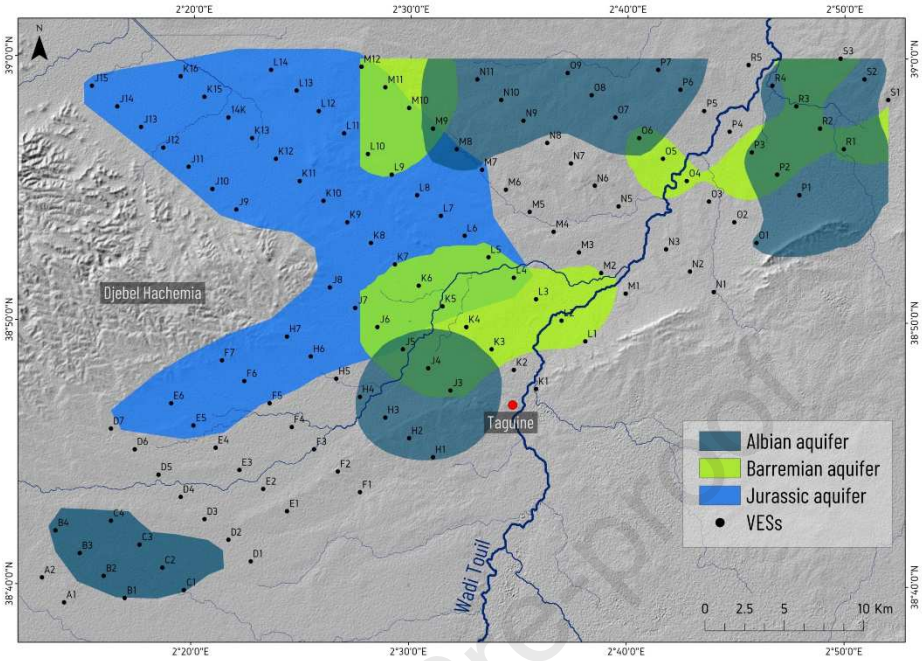

Fig.17 Suitable areas for drilling.

5. Conclusions

The use of vertical electrical sounding (VES) for groundwater potential zone detection was effectively utilized here in the semi-arid plain of Wadi Touil. The analysis of VES data through geoelectric sections and resistivity maps was used to estimate the aquifers' depth and geometry. Then according to the lithology and hydrogeological characteristics, we defined three aquifers with good water potential. The first aquifer is the combined continental intercalary aquifers (Albian + Barremian), formed mainly by sandstones. The depth of this aquifer is relatively shallow, with an average thickness of 300 m. The second important aquifer is the Jurassic formations of Kimmeridgian, which are mainly limestones with high fracture porosity. Finally, the third aquifer is the tertiary, which is less thick and with limited water production potential, but it is well distributed over the study area. The remote sensing observations were used to independently check the geophysical results by analyzing the repartition of vegetative cover in the study area. We used the remote sensing results to make the comparison between irrigated areas in 2001 and 2018, which show a net increase in farming activity in the study area, leading to an increase in water demand. Utilizing all results, a map of the most suitable drilling zones was

produced. This map provides additional information to guide decision makers when implementing new groundwater use plans.

Acknowledgments

The authors thank the four anonymous reviewers for their comments and suggestions, which improved the paper. The authors wish also to acknowledge the help received from Yougarithen Massioun for his valuable efforts during data extraction and analysis. We would like to thank Prof. Ahmed Cherif Toubal for the help during interpretation and validation of results.

References

Amri, K., Rabai, G., Benbakhti, I. M., Khennouche, M. N., 2017. Mapping geology in Djelfa District (Saharan Atlas, Algeria), using Landsat 7 ETM+ data: an alternative method to discern lithology and structural elements. Arabian Journal of Geosciences, 10(4), 87.

Aoudia, M., Issaadi, A., Bersi, M., Maizi, D., Saibi, H., 2020. Aquifer characterization using vertical electrical soundings and remote sensing: A case study of the Chott Ech Chergui Basin, Northwest Algeria. Journal of African Earth Sciences, 103920.

Asfahani, J., 2007a. Geoelectrical investigation for characterizing the hydrogeological conditions in semi-arid region in Khanasser valley, Syria. Journal of Arid Environments, 68(1), 31-52.

Asfahani, J., 2007b. Neogene aquifer properties specified through the interpretation of electrical sounding data, Salamiyeh region, central Syria. Hydrological Processes: An International Journal, 21(21), 2934-2943.

Asfahani, J., 2013. Groundwater potential estimation using vertical electrical sounding measurements in the semi-arid Khanasser Valley region, Syria. Hydrological sciences journal, 58(2), 468-482.

Ayad, A., 1991. Implantation de forages dans la vallée d'oued Touil ; ANRH Alger.

Ayad, A., 1997. Etude hydrogéologique de la plaine de Ksar Chellala ; ANRH Alger.

Barker, RD., 1989. Depth of investigation of collinear symmetrical four-electrode arrays. Geophysics, 54(8), 1031-1037.

Benabdelouahab, S., Salhi, A., Himi, M., El Messari, JES., Ponsati, AC., 2019. Geoelectrical investigations for aquifer characterization and geoenvironmental assessment in northern Morocco. Environmental Earth sciences, 78(6), 209.

Bersi, M., Saibi, H., Chabou, MC., 2016. Aerogravity and remote sensing observations of an iron deposit in Gara Djebilet, southwestern Algeria. Journal of African Earth Sciences, 116, 134-150.

Braham, M., Hamidouche, B., 2007. Étude géophysique et hydrogéologique de la plaine sud de Ksar Chellala ; mémoire d'ingénieur FSTGAT-USTHB.

Bracène, R., de Lamotte, D. F., 2002. The origin of intraplate deformation in the Atlas system of western and central Algeria: from Jurassic rifting to Cenozoic–Quaternary inversion. Tectonophysics, 357(1-4), 207-226.

Caratini, C., 1970. Geological study of the region of Chellala-Reibell. Bull, (40).

Chabane, S., Amri, K., Hamdidouche, R., 2019. Deformation pattern in the El Ahmar area (Bechar Basin, Southwestern Algeria): contribution of Lansat 8 OLI and field measurement. Arabian Journal of Geosciences, 12(5), 158.

Cimino, A., Cosentino, C., Oieni, A., Tranchina, L., 2007. A geophysical and geochemical approach for seawater intrusion assessment in the Acquedolci coastal aquifer (Northern Sicily). Environmental Geology, 55(7), 1473.

Cornet, G., 1954. Implantation de forages de reconnaissance profonds dans la région de Taguine.

Custodio, E., 2002. Aquifer overexploitation: what does it mean? Hydrogeology journal, 10(2), 254-277.

Edmunds, WM., Guendouz, AH., Mamou, A., Moulla, A., Shand, P., Zouari, K., 2003. Groundwater evolution in the Continental Intercalaire aquifer of southern Algeria and Tunisia: trace element and isotopic indicators. Applied geochemistry, 18(6), 805-822.

Famiglietti, JS., 2014. The global groundwater crisis. Nature Climate Change, 4(11), 945-948.

Fatah, B., Mohamed, B., Abdelhamid, G., 2012. Etude comparative des différentes méthodes d'estimation de l'évapotranspiration en zone semi-aride (cas de la région de Djelfa). Nature & Technology, (7), 109.

Gad, S., Kusky, T., 2007. ASTER spectral ratioing for lithological mapping in the Arabian–Nubian shield, the Neoproterozoic Wadi Kid area, Sinai, Egypt. Gondwana Research, 11(3), 326-335.

Hamimed, A., Menaa, R., Benslimane, M., Bouabdellah, L., 2008. Cartographie de l'évapotranspiration réelle journalière dans les conditions semi-arides en Algérie à partir des données satellitaires Aster. Science et changements planétaires/Sécheresse, 19(4), 293-300.

Kerbadj, N., Saibi, H., Bouzid, A., Bounif, MO., Bougchiche, S., 2017. 2-D inversion of magnetotelluric data at Dar-Chioukh region (Djelfa, Algeria). The 4th International Conference on Engineering Geophysics (ICEG), Al-Ain, UAE, 9-12 October 2017.

Khezzani, B., Bouchemal, S., 2018. Variations in groundwater levels and quality due to agricultural over-exploitation in an arid environment: the phreatic aquifer of the Souf oasis (Algerian Sahara). Environmental earth sciences, 77(4), 142.

Kosinski, WK., Kelly, WE., 1981. Geoelectric soundings for predicting aquifer properties. Groundwater, 19(2), 163-171.

Laouisset, MB., Dellal, A., 2016. Estimation of Barley (Hordeum Vulgare L.) Crop Water Requirements Using Cropwat Software in Ksar-Chellala Region, Algeria. Agris on-line Papers in Economics and Informatics, 8(665-2016-45099), 91-102.

Lasaponara, R., 2006. On the use of principal component analysis (PCA) for evaluating interannual vegetation anomalies from SPOT/VEGETATION NDVI temporal series. Ecological modelling, 194(4), 429-434.

Madani, A. A., Emam, A. A., 2011. SWIR ASTER band ratios for lithological mapping and mineral exploration: a case study from El Hudi area, southeastern desert, Egypt. Arabian journal of Geosciences, 4(1-2), 45-52.

Mamou, A., Besbes, M., Abdous, B., Latrech, DJ., Fezzani, C., 2006. North Western Sahara Aquifer System (NWSAS). Into the well from which you drink do not throw stones, 68.

Maoui, A., Kherici, N., Derradji, F., 2010. Hydrochemistry of an Albian sandstone aquifer in a semi arid region, Ain oussera, Algeria. Environmental earth sciences, 60(4), 689-701.

Maury, S., Balaji, S., 2014. Geoelectrical method in the investigation of groundwater resource and related issues in Ophiolite and Flysch formations of Port Blair, Andaman Island, India. Environmental earth sciences, 71(1), 183-199.

Metwaly, M., Elawadi, E., Moustafal, SS., Al Fouzan, F., Mogren, S., Al Arifi, N., 2012. Groundwater exploration using geoelectrical resistivity technique at Al-Quwy'yia area central Saudi Arabia. International Journal of Physical Sciences, 7(2), 317-326.

Mohamed, H., Saibi, H., Bersi, M., Abdelnabi, S., Geith, B., Ismaeil, H., Tindell, T., Mizunaga, H., 2018. 3-D magnetic inversion and satellite imagery for the Um Salatit gold occurrence, Central Eastern Desert, Egypt. Arabian Journal of Geosciences, 11(21), 674.

Mozas, M., Ghosn, A., 2013. État des lieux du secteur de l'eau en Algérie. Institut de Perspective Économique du Monde Méditerranéen (IPMED).

Nejad, HT., Mumipour, M., Kaboli, R., Najib, OA., 2011. Vertical electrical sounding (VES) resistivity survey technique to explore groundwater in an arid region, Southeast Iran. Journal of applied sciences, 11(23), 3765-3774.

Redhaounia, B., Aktarakçi, H., Ilondo, BO., Gabtni, H., Khomsi, S., Bédir, M., 2015. Hydro-geophysical interpretation of fractured and karstified limestones reservoirs: A case study from Amdoun region (NW Tunisia) using electrical resistivity tomography, digital elevation model (DEM) and hydro-geochemical approaches. Journal of African Earth Sciences, 112, 328-338.

Richey, AS., 2014. Stress and Resilience in the World's Largest Aquifer Systems: A GRACE-based methodology. UC Irvine.

Roy, A., Apparao, A.,1971. Depth of investigation in direct current methods. Geophysics, 36(5), 943-959.

Roy, KK., Elliot, HM., 1981. Some observations regarding depth of exploration in DC electrical methods. Geoexploration, 19(1), 1-13.

Saibi, H., Bersi, M., Mia, MB., Saadi, NM., Al Bloushi, KM., Avakian, RW., 2018. Applications of Remote Sensing in Geoscience. Recent Advances and Applications in Remote Sensing. 2018 Jul 25:181.

Sikandar, P., Christen, E., 2012. Geoelectrical sounding for the estimation of hydraulic conductivity of alluvial aquifers. Water resources management, 26(5), 1201-1215.

Torbick, N., Becker, B., 2009. Evaluating principal components analysis for identifying optimal bands using wetland hyperspectral measurements from the Great Lakes, USA. Remote Sensing, 1(3), 408-417.

Winn, RM., 1973. Hydrogeology of the Albian Formation, Algeria. Texas Tech University.

Yadav, G., Singh, SK., 2007. Integrated resistivity surveys for delineation of fractures for ground water exploration in hard rock areas. Journal of applied geophysics, 62(3), 301-312.

Zaidi, FK., Kassem, OMK., 2012. Use of electrical resistivity tomography in delineating zones of groundwater potential in arid regions: a case study from Diriyah region of Saudi Arabia. Arabian Journal of Geosciences, 5(2), 327-333.

Figure captions

Fig. 1 General location map of the Wadi Touil plain showing the vertical electrical soundings location.

Fig. 2 A Geological map of the study area, modified after (modified from Cornet (1954)), B: Synthetic stratigraphic log.

Fig.3 Distribution map of the vertical electrical soundings and boreholes in the study area.

Fig. 4 Principle of electrical method. Electrical current is injected at A and B electrodes. Difference in potential is measured between M and N electrodes.

Fig. 5 Calibration of four standard VES surveys using four boreholes.

Fig. 6 Synthetic resistivity scale in the study area.

Fig. 7 Methodological approach.

Fig. 8 Isoapparent resistivity maps showing the subsurface geo-electrical structure of the study area.

Fig. 9 D profile pseudo section and geoelectrical section.

Fig.10 K profile pseudo section and geoelectrical section.

Fig. 11 M profile pseudo section and geoelectrical section.

Fig. 12 P profile pseudo section and geoelectrical section.

501 Fig. 13 Isodepth and isopach maps of Albian and Barremian aquifers. A) Isodepth map of the Albian aquifer. B)
502 Isopach map of the Albian aquifer. C) Isodepth map of the Barremian aquifer. D) Isopach map of the Barremian
503 aquifer.

504 Fig. 14 Best aquifer geometry and promising zones.

505 Fig. 15 PCA map showing vegetation density and repartition in 2001 and 2018.

506 Fig. 16 Red/NIR Ratios map showing irrigated areas.

507 Fig.17 Suitable areas for drilling.

508

Highlights

- Identification of three potential aquifers from the variation of electric resistivity.
- Determination of depth and thickness of the continental intercalary aquifer in the Wadi Touil Plain.
- Contribution to the decision making regarding the favorable sites for drilling purposes.

Declaration of interests

☒ The authors declare that they have no known competing financial interests or personal relationships that could have appeared to influence the work reported in this paper.

☐The authors declare the following financial interests/personal relationships which may be considered as potential competing interests: